Available online at www.sciencedirect.com
SCIENCE DIRECT
Applied Catalysis A: General 287 (2005) 147–158
APPLIED CATALYSIS A: GENERAL
www.elsevier.com/locate/apcata

A stable, novel catalyst improves hydrogen production in a membrane reactor

S. Irusta, J. Múnera, C. Carrara, E.A. Lombardo, L.M. Cornaglia *

Instituto de Investigaciones en Catálisis y Petroquímica (FIQ, UNL-CONICET), Santiago del Estero 2829, 3000 Santa Fe, Argentina

Received 22 December 2004; received in revised form 11 March 2005; accepted 14 March 2005
Available online 17 May 2005

Abstract

The dry reforming of methane as a source of H_2 was performed using a well-known catalyst, Rh/La_2O_3, together with a novel one, Rh/La_2O_3-SiO_2, in a hydrogen-permeable membrane reactor. The catalysts were characterized by XRD, TPR, FTIR, H_2 and CO chemisorption. In all lanthanum-based catalysts, the activity remained constant after 100 h on stream at 823 K. The basis of their high stability could be traced back to the strong metal-support interaction (TPR) in Rh/La_2O_3 catalysts. The La_2O_3-SiO_2 solids are also stable even though a weaker rhodium–lanthanum interaction (TPR) can be observed. The incorporation of the promoter (La_2O_3) to the silica support induces a parallel increase in the metal dispersion (CO adsorption). The effect of the operation variables upon the performance of the membrane reactor was also studied. The novel Rh (0.6%)/La_2O_3 (27%)-SiO_2 catalyst proved to be the best formulation. Operating the membrane reactor at 823 K, both methane and CO_2 conversions were 40% higher than the equilibrium values, producing 0.5 mol H_2/mol CH_4. This catalyst, tested at W/F three times lower than Rh (0.6%)/La_2O_3, showed a similar performance. Both the increase of the sweep gas flow rate and the decrease of the permeation area significantly affected methane conversion and H_2 production. The presence of tiny amounts of graphite only detectable through LRS did not endanger membrane stability. The better performance of Rh (0.6%)/La_2O_3 (27%)-SiO_2 is related to the high dispersion.

Keywords: Membrane reactor; Hydrogen production; Rh catalysts; La_2O_3-SiO_2; CO_2 reforming

1. Introduction

The dry reforming of methane as a source of H_2 was performed using a commercial Ni catalyst and supported Ru, Pd, Ir and Pt formulations in hydrogen-permeable membrane reactors. The main problems encountered in this application were the abundant formation of coke, deleterious to the membrane [1], and catalyst deactivation. Appropriate catalysts preventing the formation of carbon deposits are needed to avoid membrane damage.

The membrane reactors employed for the reforming reaction were based on different membrane types such us porous [2], catalytic porous [3], silica modified vycor [4], and thin palladium film [5]. In previous studies [6,7], we reported that CH_4 conversion can be greatly improved by removing the hydrogen formed with a stable and highly selective Pd–Ag dense membrane. The rhodium catalysts supported on lanthanum were active and stable for the dry reforming reaction despite the low dispersion of the metal.

Vidal et al. [8] reported dispersion values as high as 100% in Rh catalysts when a composite La_2O_3-SiO_2 solid was used as support. A higher metal dispersion could lead to increased activity in the dry reforming; a better performance of the membrane reactor would consequently be obtained.

Infrared spectra of adsorbed carbon monoxide can give valuable information about surface sites in mixed metal catalysts [9]. Experimental information is available for CO adsorption on Rh particles supported on various oxide supports [10]. Knözinger and co-workers [11] studied the metal state on promoted Rh/SiO_2 catalysts, finding that $Rh(CO)_2^+$ cations sit on the respective promoter oxide in $Rh/X/SiO_2$ (X = Ta, Nb or V). The SMSI state as induced by high temperature (HT) reduction gave rise to changes in the

* Corresponding author. Present address: College of Chemical Engineering Physicalchemistry, Sgo del Estero 2829, 3000 Santa Fe, Argentina. Tel.: +54 3424536861; fax: +54 3424536861.
E-mail address: lmcornag@fiqus.unl.edu.ar (L.M. Cornaglia).

0926-860X/$ – see front matter
doi:10.1016/j.apcata.2005.03.018

relative amount of linearly to bridge-bonded CO. Bernal et al. [12] used FTIR spectroscopy of CO adsorbed on Rh/La_2O_3/SiO_2 to obtain information about the influence of the preparation procedure on the chemical behavior of these samples.

In this work, we report the results obtained with a novel catalyst, Rh/La_2O_3-SiO_2, and with Rh/La_2O_3. The fresh catalysts were characterized by XRD, TPR, FTIR and CO and hydrogen chemisorption. FTIR spectroscopy with CO as a probe molecule was used to study the promoter oxide role. The effect of the operation variables and the catalyst activity upon the performance of the membrane reactor was also studied.

2. Experimental

2.1. Catalyst preparation

The SiO_2 (Aerosil 300) employed in the solid preparation was previously calcined at 1173 K. The La_2O_3-SiO_2 support was prepared by incipient wetness impregnation of SiO_2 with lanthanum nitrate (Anedra). Two different La loadings were used (7 and 27.0 wt.% of La_2O_3). The solids were calcined at either 873 or 1173 K. Metal deposition was performed with $RhCl_3 \cdot 3H_2O$ (Alfa) as precursor compound. The Rh/La_2O_3-SiO_2 and Rh/SiO_2 catalysts were prepared by incipient wetness impregnation. The samples were kept at room temperature for 4 h and then dried at 343 K overnight. The Rh/La_2O_3 solids were obtained by wet impregnation of lanthanum oxide (Anedra 99.99%) with two different Rh contents (0.2 and 0.6 wt.%). The resulting suspension was then heated at 353 K to evaporate the water and the solid material was dried in an oven at 383 K overnight. All the catalysts were calcined in flowing air at 823 K during 6 h.

A BET surface area of approximately 180 g m^{-2} was measured for all La_2O_3-SiO_2 catalysts and supports.

2.2. X-ray diffraction (XRD)

The XRD patterns of the solids were obtained with an XD-D1 Shimadzu instrument, using Cu Kα radiation at 35 kV and 40 mA. The scan rate was 1° min^{-1} in the range $2\theta = 10°$–$80°$.

2.3. Temperature-programmed reduction (TPR)

An Ohkura TP-20022S instrument equipped with TCD was used for the TPR experiments. To eliminate the carbonates present in the samples, the following pre-treatments were used: the samples were heated up to 823 K in oxygen flow, kept constant for half an hour and then cooled down in Ar flow. Afterwards, they were reduced in a 5%H_2-Ar stream, with a heating rate of 10 K min^{-1} up to the maximum treatment temperature.

2.4. Metal dispersion

The Rh dispersion of the fresh catalysts, following the H_2 reduction at 773 K for 2 h, was determined by static equilibrium of either H_2 or CO adsorption at room temperature in a conventional vacuum system. The CO uptakes were calculated taking into account the three adsorption states (linear, bridge and gem) construction. The contribution of each one was evaluated by a fit of the FTIR bands using Lorentzian functions. The integral extinction coefficients and stoichiometric factors were taken from Knözinger and co-workers [11].

2.5. FT infrared spectroscopy (FTIR)

The IR spectra were obtained using a Shimadzu FTIR 8101 M spectrometer with a spectral resolution of 4 cm^{-1}. The solid samples were prepared in the form of pressed wafers (ca. 2 wt.% sample in KBr). The samples for the CO adsorption experiments were prepared by compressing the pure solids at 2 tonnes cm^{-2} in order to obtain a self-supporting wafer (50 mg, 10 mm diameter). They were mounted in a transportable infrared cell with CaF_2 windows and external oven. The pre-treatment was performed in a high vacuum system. The samples were first reduced at 723 K during 1 h in flowing H_2 and then outgassed for 1 h at 723 K in a dynamic vacuum of 7×10^{-4} Pa. After cooling to room temperature, a spectrum of the catalyst wafer was taken. After that, 1.6×10^4 Pa of CO were admitted into the cell, left in contact with the solid for 10 min, and then a spectrum was recorded. Spectra were also recorded after heating at 473 K and evacuation of the cell for 10 min at 298 and 373 K.

2.6. Temperature-programmed desorption (TPD)

TPD measurements were carried out on the calcined samples. The temperature was increased at 10 K min^{-1} from 300 to 1073 K. The final temperature was kept constant for 2 h. The evolved gases were analyzed by a ThermoStar Balzer quadrupole mass spectrometer.

2.7. Catalytic test

2.7.1. Fixed-bed reactor

The catalyst (50 mg) was loaded into a tubular quartz reactor (inner diameter, 5 mm) which was placed in an electric oven. A thermocouple in a quartz sleeve was placed on top of the catalyst bed. The catalysts were heated in He at 973 K and then reduced in situ in H_2 at the same temperature for 2 h. After reduction, the temperature was adjusted in flowing He to the reaction temperature (823–973 K); and the feed gas mixture (33% CH_4, v/v, 33% CO_2, 34% He, $P = 1$ atm) was switched to the reactor. The stability tests were carried out at $W/F = 2.67 \times 10^{-5}$ g h ml^{-1}; conver-sion was measured at $W/F = 4.5 \times 10^{-6}$ g h ml^{-1}.

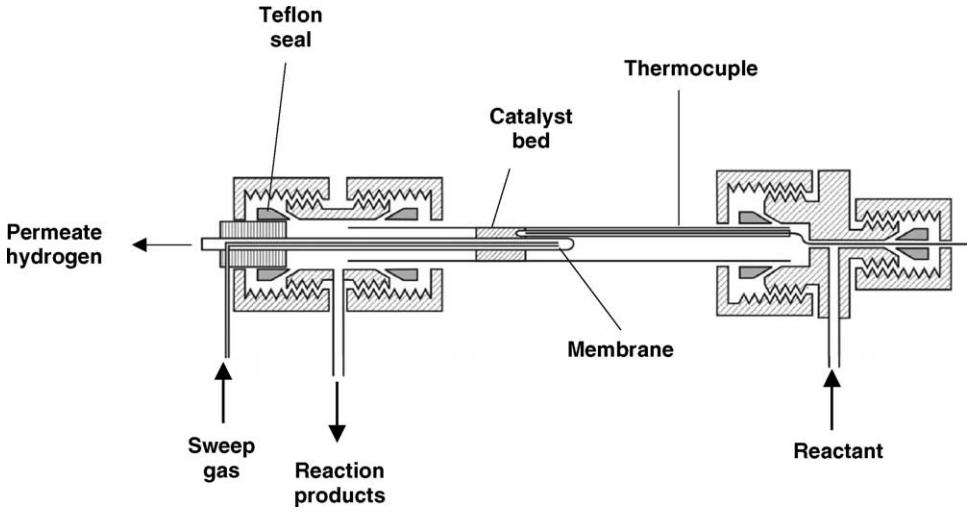

Fig. 1. Membrane reactor scheme.

The reaction products were analyzed in a TCD gas chromatograph (Shimadzu GC-8A) equipped with a Porapak column, and a molecular sieve column.

2.7.2. Membrane reactor

The double tubular membrane reactor was built using a commercial dense Pd–Ag alloy (inner tube), provided by REB Research and Consulting, with one end closed and an inner tube to allow helium sweep gas flow. The outer tube was made of commercial non-porous quartz (i.d. 9 mm). The catalyst, diluted with quartz chips to obtain the 3 cm bed height, was packed in the outer annular region (shell side). The inner side of the membrane in all runs was kept at atmospheric pressure. The reactor scheme is shown in Fig. 1. More details were previously reported [6]. The catalysts were heated in He at 823 K and then reduced in situ in H_2 at the same temperature for 2 h. After reduction, the feed stream gas mixture (33%CH_4, v/v, 33% CO_2, 34% He, $P = 1$ atm) was switched through the reactor.

In order to measure the equilibrium conversions, the membrane reactor was operated with neither sweep gas nor pressure difference between the tube and the shell sides. The conversions were measured after a 12-h stabilization period.

3. Results and discussion

3.1. Reaction rates and stability of the Rh solids

Activity and stability tests were performed on Rh catalysts supported on lanthanum oxide and La_2O_3-SiO_2 mixed oxides in a fixed-bed reactor. Methane and carbon dioxide initial reaction rates are presented in Table 1. The activity after 100 h on stream was monitored in the same tests and the measured reaction rates (Table 1) showed the high stability of all the lanthanum solids.

The La_2O_3-SiO_2-based samples were also tested without solid calcination; a slight decrease in the initial reaction rate of methane at 823 K was observed. The catalysts supported on La_2O_3-SiO_2 exhibited reaction rates higher than those supported on lanthanum oxide.

Table 1
Catalytic performance of Rh solids in a fixed-bed reactor

Catalysts[a]	TOF_{CH_4}[b] (s^{-1})	r_{CH_4}[b] (mol h^{-1} g^{-1})	r_{CO_2}[b] (mol h^{-1} g^{-1})	r_{CH_4}[c] (mol h^{-1} g^{-1})	r_{CO_2}[c] (mol h^{-1} g^{-1})	Dispersion
Rh (0.2%)/La_2O_3	3.6	0.16	0.33	0.16	0.32	0.64[d]
Rh (0.6%)/La_2O_3	6.1	0.18	0.45	0.18	0.44	0.14[d]
Rh (0.6%)/SiO_2	11.3	0.19	0.43	–	–	0.08[d]
Rh (0.6%)/La_2O_3 (7%)SiO_2 (873 K) La/Rh = 7.4	3.2	0.34	0.66	0.34	0.56	0.51[e]
Rh (0.6%)/La_2O_3 (27%)SiO_2 (873 K) La/Rh = 28.6	1.8	0.30	0.61	0.33	0.64	0.79[e]
Rh (0.6%)/La_2O_3 (27%)SiO_2 (1173 K) La/Rh = 28.6	4.0	0.31	0.71	0.32	0.71	0.37[e]

[a] Solids were reduced in situ at 823 K before reaction. The wt.% of Rh and La_2O_3 are given between parentheses. The La_2O_3-SiO_2 supports were calcined at 873 or 1173 K as is indicated between parentheses.
[b] Initial reaction rates measured at 823 K.
[c] Reaction rates measured at 823 K, $W/F = 1.05 \times 10^{-5}$ g h ml^{-1}, after 100 h on stream.
[d] Obtained by H_2 chemisorption.
[e] Obtained by CO chemisorption.

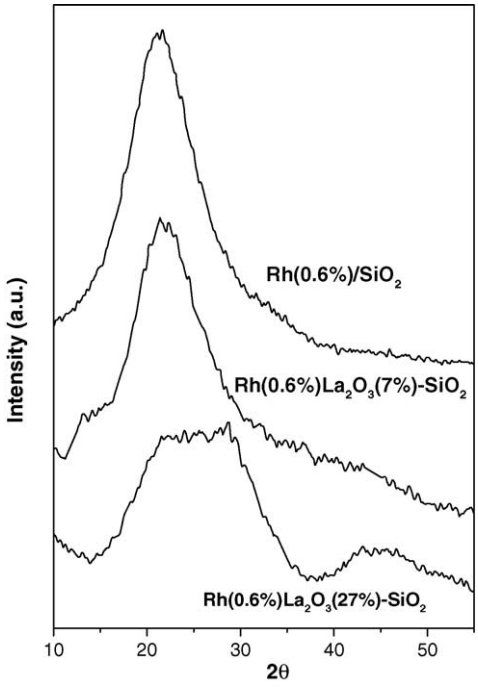

Fig. 2. XRD patterns of the Rh (0.6%) supported on SiO_2 and La_2O_3-SiO_2. La_2O_3-SiO_2 supports calcined at 873 K.

3.2. Bulk characterization of the solids

Fig. 2 shows the diffraction patterns of the La_2O_3-SiO_2 catalysts. For the Rh (0.6%)/SiO_2 sample, the XRD pattern is similar to pure SiO_2 support calcined at 1173 K (not shown). However, the Rh (0.6%)La_2O_3 (27%)/SiO_2 pattern shows a significant broadening that corresponds to the appearance of the characteristic peaks of lanthanum disilicate phase $La_2Si_2O_7$ at $2\theta = 28^\circ$ and 45° as was previously reported by Vidal et al. [13]. For the low La_2O_3 loading catalyst (Rh (0.6%)La_2O_3 (7%)/SiO_2) these peaks are very weak. The sample calcined above 1173 K presents no differences in the diffraction patterns compared to Rh (0.6%)La_2O_3 (27%)SiO_2 calcined at 873 K. Peaks indicating the presence of lanthanum carbonates, oxycarbonates or hydroxide were not observed.

In previous studies [7,14] we reported the characterization of crystalline phases on the lanthanum support and the Rh and Pt catalysts by laser Raman spectroscopy, FTIR, XRD, TPD and TGA. The support and the calcined fresh catalysts exhibited a mixture of phases which were influenced by the metal type. Catalysts with a low rhodium loading showed an increase of Ia-$La_2O_2CO_3$ already present on the support, whereas those with a low platinum loading would not modify the phases of the lanthanum solid. However, the only remaining crystalline phase after 100 h on stream was II-$La_2O_2CO_3$.

The main gaseous products obtained in the desorption experiments carried out in the La_2O_3 supported catalyst were CO_2 and H_2O. This solid had a high proportion of Ia-oxycarbonate in the support composition [14]. For the Rh (0.6%)/La_2O_3 (7%)-SiO_2 solid, the 44 amu profile displayed one peak at 573 K while the 18 amu showed a peak at 523 K with a shoulder at 573 K. These results (not shown) revealed the presence of $La(OH)_3$ and hydroxycarbonate in the solid with low loading of lanthanum; however, the TPD of solids with 27% La_2O_3 did not show desorption of CO_2 and H_2O.

On the other hand, the FTIR spectra (not shown) of all the La_2O_3-SiO_2 solids showed only the fingerprints of SiO_2. Bands at 1470 and 1393 cm^{-1} that were observed in the catalyst with 7% of La_2O_3 in the support could be assigned to lanthanum hydroxide in agreement with the TPD results. The lanthanum disilicate detected through XRD could prevent the formation of detectable amounts of lanthanum oxycarbonates or hydroxide in the case of high La loading supports even after a long time on stream.

Interesting changes occurred in the spectra in the region of stretching and combination vibrations of –OH and –SiOH groups due to the presence of lanthanum. For reduced and then evacuated solids, the signal at 3744 cm^{-1} was obtained, universally assigned to an isolated surface OH group unperturbed by its neighbours. Besides, the development of a shoulder at 3738 cm^{-1} was observed in the supports with 7 and 27% La_2O_3. Vidal et al. [8] in similar La-Si solids also found a shoulder at a lower wavenumber; in both cases it can be attributed to hydrogen-bonded OH groups.

3.3. Reducibility of catalysts based on different lanthanum supports

3.3.1. Non-pretreated calcined samples

The TPR profiles of the untreated La_2O_3(27%)-SiO_2 samples show two peaks at 403 and 545 K (Table 2 and Fig. 3a). They exhibit a total hydrogen consumption (H_2/Rh = 2.7) higher than the normal value (taking into account the reduction of the Rh_2O_3 to Rh°), due to the appearance of a second peak at approximately 540 K. The same experiment was performed employing a mass spectrometer as detector. Only the 16 mass desorption corresponding to water was observed at 500 K.

After the TPR experiment, the reoxidation of the Rh (0.6%)/La_2O_3 (27%)SiO_2 sample was carried out with flowing oxygen at 823 K. The TPR profile of the reoxidized sample gave a normal hydrogen consumption (H_2/Rh = 1.5), suggesting that the second peak (540 K) was due to a desorption process. Borer and Prins [16] using mass spectrometry analysis showed that the TPR peak above 500 K of the unpretreated LaRh solids was connected with the evolution of CH_4 around 540 K. Bernal and co-workers [8] found that the carbonated phase on Rh/La_2O_3 decomposed during reduction in two steps at 573 and 723 K, respectively, while carbonated La_2O_3 decomposed at 800 K. Borer and Prins [16] assumed that methane was originated from carbonated lanthanum species. Even though fresh Rh/La_2O_3 catalysts exhibit a mixture of carbonate phases [7], none of these phases were detected on the La_2O_3-SiO_2 supported solids by FTIR, XRD or LRS except for the solid

Table 2
TPR data of the calcined Rh solids

Catalysts	Untreated[a]		Pre-treated[b]	
	H_2/Rh[c]	T_{max} (K)	H_2/Rh[c]	T_{max} (K)
Rh (0.2%)/La_2O_3	–	–	0.82	433, 490
Rh (0.6%)/La_2O_3	–	–	1.40	423, 451
Rh (0.6%)/SiO_2	1.35	382–415	1.28	374
	1.00	600 w–680 w[e]		421 w
Rh (0.6%)/La_2O_3 (7%)SiO_2 (873 K) La/Rh = 7.4	18.0	490–513	1.98	421
Rh (0.6%)/La_2O_3 (27%)SiO_2 (873 K) La/Rh = 28.6	2.66	403, 545 vs[e]	1.47	420
Rh (0.6%)/La_2O_3 (27%)SiO_2 (873 K) La/Rh = 28.6	–	–	1.41[d]	417[d]
Rh (0.6%)/La_2O_3 (27%)SiO_2, 1173 K La/Rh = 28.6	2.84	401, 539 vs[e]	1.12	420

[a] Without in situ treatment.
[b] Pre-treated in O_2 flow at 823 K in the TPR instrument.
[c] μmol H_2/μmol metal ratio.
[d] Reoxidized sample after the first TPR experiment of the untreated sample.
[e] w: weak; vs: very strong.

with 7% lanthana (TPD results). In this case, the decomposition of hydroxycarbonate would produce CH_4 and it could be related to the very strong TPR peaks (H_2/Rh = 18.0).

Vidal et al. [8] studied the reducibility of the uncalcined Rh/La-Si catalyst and assigned the reduction peak at 450 K to the reduction of species generated in the lanthana redissolution process. This peak was lower for the support calcined at high temperature. Bernal et al. [12] suggested that the impregnation of the LaSi system, previously calcined at 873 K with an aqueous solution of Rh nitrate, induces the leaching of the lanthanum containing phase. They sustained that calcination at 1173 K would prevent the leaching of the phase. These results agree well with the lower intensity of the second TPR peak in our Rh (0.6%)/La_2O_3 (27%)SiO_2 profile.

3.3.2. *In situ oxygen pre-treatment*

To release the adsorbed water and CO_2, the samples were pre-treated in the TPR flow system. After treatment in flowing oxygen at 823 K, the Rh catalysts supported on lanthanum oxide showed two main peaks between 420 and 490 K (Table 2, Fig. 3b), independently of the Rh loading. A weak shoulder was observed at 405 K. On the other hand, the Rh/SiO_2 system exhibits the most intense reduction peak at 374 K. The reduction temperature in the Rh/La_2O_3 catalysts, which was significantly higher than in the SiO_2 solid, indicates that there is an important interaction between rhodium and the La_2O_3 support [15].

An intermediate situation occurs with the Rh supported on La_2O_3-SiO_2: the TPR profiles show a sharp single peak at 420 K independent of La_2O_3 loading (Fig. 3b). A smaller change in the reduction temperature is observed.

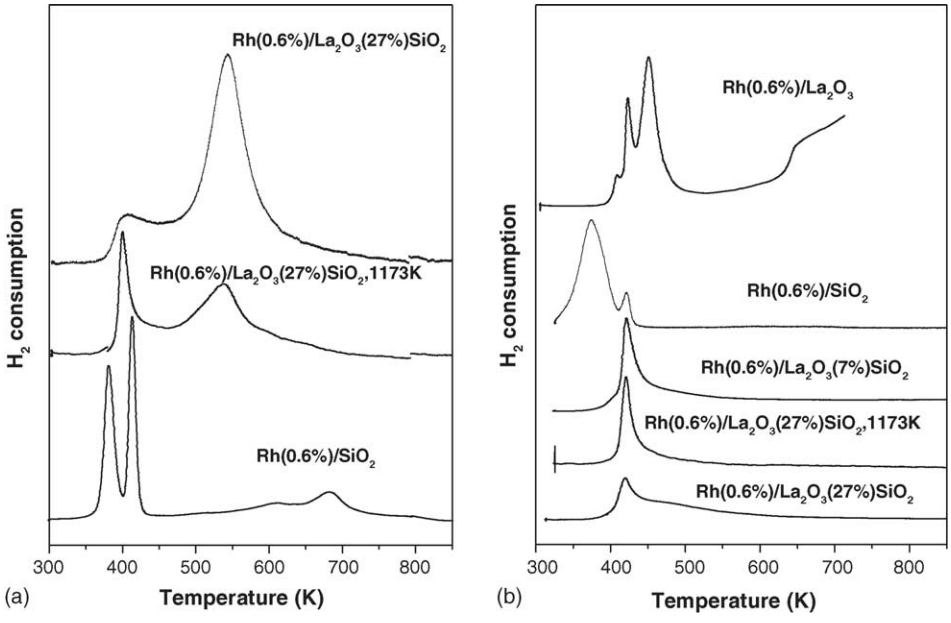

Fig. 3. TPR profiles of calcined Rh catalysts: (a) untreated; (b) pre-treated in oxygen flow at 823 K in the TPR instrument.

Borer and Prins [16] studied the reducibility of the Rh-La-Si catalysts prepared by wet impregnation and using nitrate impregnation salts. They found higher TPR peak temperatures with increasing La content, due to the stabilization effect of La_2O_3 which decreases Rh_2O_3 reducibility. Increasing the La content also led to a higher hydrogen consumption. They explained this behavior by the partial reduction of the lanthanum oxide as proposed by other authors.

In our incipient wetness prepared catalysts, no changes were observed in the reduction peak temperature with lanthanum loading. The hydrogen consumption was almost the same for all samples using supports calcined at 873 K. When the support was calcined at 1173 K, a lower H_2/Rh was measured.

It is important to remark that these previous papers employed rhodium nitrate as impregnation salt but in our case we used rhodium trichloride. It has been reported [17] that metal catalysts derived from chloride precursors could form larger metal particles.

3.4. CO adsorption

It is well known that the FTIR spectrum of CO-Rh is characterized by three main kinds of species: (1) $Rh^+(CO)_2$ gem-dicarbonyls associated with a doublet at 2090–2100 cm^{-1} and 2016–2034 cm^{-1} due to asymmetric and symmetric stretching [18]; (2) linearly bonded CO characterized by a single band at 2060–2075 cm^{-1}; and (3) bridged CO, the characteristic features of which appear in the 1850–1925 cm^{-1} region [12].

3.4.1. Adsorption at 300 K

The spectrum of the Rh (0.6%)/La_2O_3 catalyst (Fig. 4) contains a band at 2050 cm^{-1} due to linearly adsorbed CO on Rh but no evidence for bands due to gem-dicarbonyl or bridged CO complex. Following the spectral changes in time (2 h) in the presence of CO, the appearance of weak dicarbonyl bands at 2095 and 2010 cm^{-1} was observed. Evacuation at 300 K led to a decrease in the intensity of these bands and a small change at 2050 cm^{-1}. The total desorption of CO occurred when the sample was evacuated at 373 K.

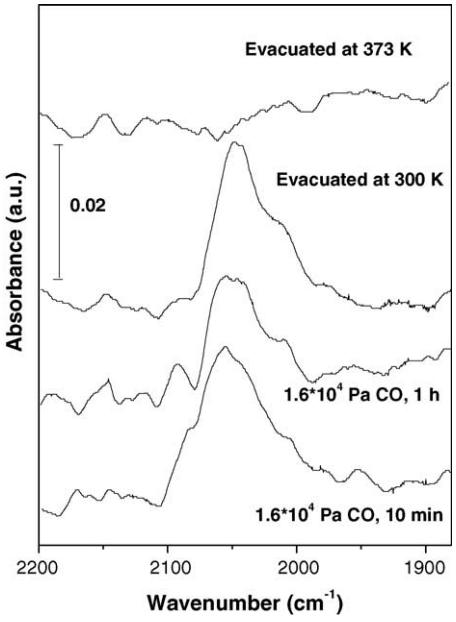

Fig. 4. FTIR spectra of the ν_{CO} region of Rh (0.6%)/La_2O_3.

The spectrum of CO adsorbed on Rh (0.6%)/SiO_2 at room temperature shows one band at 2062 cm^{-1} that is attributed to terminally bonded CO, while the broad band at 1919 cm^{-1} is due to the bridge-bonded CO (Fig. 5). These two kinds of chemisorbed species are the first ones to appear at low CO pressure exposures ($<4 \times 10^4$ Pa CO) [9,18]. Knözinger and co-workers [11] working with 10 kPa CO at 85 K also found linearly and bridged CO species, as dominant features. Dumesic and co-workers [10] pointed

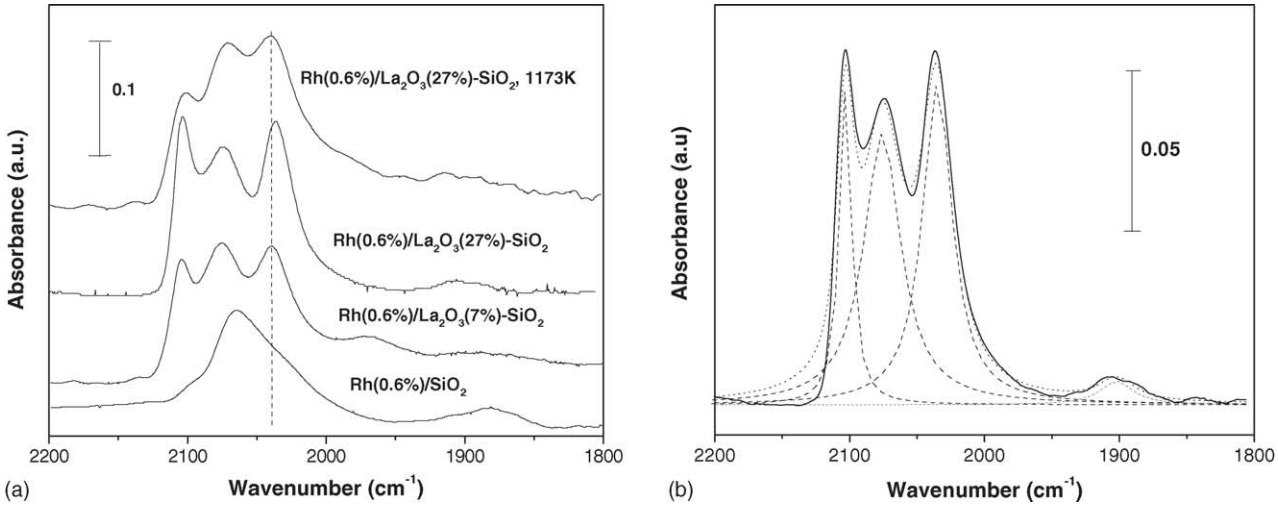

Fig. 5. FTIR spectra after exposure to 1.6×10^4 Pa CO at 298 K (a) Rh catalysts; (b) curve fitted spectrum of bridge, linear and dicarbonyl CO on the Rh (0.6%)/La_2O_3 (27%)-SiO_2 solid.

out that the absence of dicarbonyl species on Rh/SiO_2 catalysts may in part be due to the fact that these species are not favored on silica.

Addition of 7 and 27% of lanthanum to the silica support caused a shift of 13 cm^{-1} to a higher wavenumber on the stretching frequency of linearly bonded CO (Fig. 5). The modification of Rh/SiO_2 with promoter oxides (V, Nb and Ta) was found to cause a slight blue-shift of the bands pertaining to linear CO on rhodium. This shift was ascribed to a particle size effect as smaller particles exhibit a higher fraction of edge and corner atoms, which are electron deficient [11]. Additionally, the promoter oxide may electronically influence the stretching frequency of linearly bonded CO by polarization of small metal clusters [19]. On the other side, the lower IR frequency of CO on Rh-Te silica supported solids [10] compared to Rh/SiO_2 was said to be partially caused by a less significant dipole–dipole coupling between neighbouring CO molecules, in view of the larger separation between absorbates on the Rh-Te catalysts. All these effects could be responsible for the band shift in our catalysts and would be related to the high Rh dispersion observed.

The dicarbonyl species are formed from highly dispersed metallic rhodium by virtue of an oxidation process involving isolated acidic OH groups of the support. This reaction requires the existence of mobile CO-Rh° intermediate species [20]. Twin band intensities clearly increase with lanthanum content (Fig. 5a, Table 3), suggesting that the oxidative disruption process is favored by the presence of lanthanum on the support. The solid calcined at high temperature (1173 K) shows a lower concentration of dicarbonyl species (Table 3). The particles of Rh formed in this support would be less reactive against the OH groups. On lanthanum promoted Rh/SiO_2, Bernal et al. [12] found important gem-dicarbonyl bands in the sample with the highest rhodium dispersion. In our solids the incorporation of the promoter to the silica support induced a parallel increase in the metal dispersion (Table 3).

The rhodium dicarbonyl complex may be located directly on the promoter oxide or on silica oxygens which are electronically modified by adjacent promoter oxides. In the latter case, not only the carbonyl stretching frequency of the $Rh^{+}(CO)_2$ but also the O–H frequency of residual silanol groups would be affected [11]. In our solids no shift of twin bands could be observed because only linearly adsorbed CO occurred on the SiO_2 supported solid. There was no shift of the perturbed O–H stretching frequency of silanol groups upon adsorption of CO (not shown), so it can be inferred that $Rh^{+}(CO)_2$ cations are located on the promoter.

The band structure of bridging CO ligands was found to change upon promotion [11]. The disappearance of the band at 1920 cm^{-1} in promoted catalysts suggests that these sites are modified by the promoter oxide. These changes were ascribed to the inhibition of Rh° surface reconstructions and to particle size effects. The band of bridge-bonded CO at 1890 cm^{-1} observed in the Rh (0.6%)/SiO_2, that may be assigned to $Rh_2(CO)_3$ [9], shifted to 1995 cm^{-1} in the solid with 7% lanthanum and to 1900 cm^{-1} in the Rh (0.6%)/La_2O_3(27%)-SiO_2. These bands at higher wavenumbers are also probably due to the bridging CO complex [9]. The change in the band of bridge-bonded CO on Rh° depends on the load of La_2O_3. The effect of the promoter could be ascribed to morphological changes of the surface of rhodium particles and/or to particle size effects [11].

In order to further analyze the spectra, bands characteristic of the three adsorption states of CO were decomposed and their integrated intensities were measured (Fig. 5b); the results are shown in Table 3. In order to correct deviation in the wafer thickness the signal intensities were normalized to the pellet weight [11]. The concentration of surface Rh atoms slightly increases with the presence of lanthanum. This is consistent with the high Rh dispersion.

On the other hand, the support calcined at 1173 K presents a Rh surface concentration even lower than that of the unpromoted solid. The total CO chemisorption capacity was found to be lowered by the SMSI in oxide promoted Rh/SiO_2 catalysts [11]. For Rh/La_2O_3 catalysts, Rb promotion resulted in a decoration of the crystalline surface leading to a partial suppression of CO chemisorption [21]. The low CO adsorption (low dispersion value and low surface concentration) of the high temperature calcined solid could be associated to a higher rhodio–lanthanum interaction and/or to a partial decoration of the metal particles by the lanthanum phase.

The (linear to bridge) L/B ratio is slightly higher in the solids with lanthana (Table 3). Knözinger and co-workers [11] also observed the same phenomenon on Rh/Nb and Rh/Ta supported on SiO_2. These results were explained by a

Table 3
CO adsorbed on reduced catalysts at 300 K[a]

Catalyst	%L[b]	%G[c]	%B[d]	$C_{Rh,total}$ (10^{-9} mol cm^{-1})	L/B
Rh (0.6%)/SiO_2	90.0	1.3	8.7	6.5	10.2
Rh (0.6%)/La_2O_3 (7%)-SiO_2	84.5	9.2	6.3	8.9	13.3
Rh (0.6%)/La_2O_3 (27%)-SiO_2	80.0	14.2	5.8	8.9	13.6
Rh (0.6%)/La_2O_3 (27%)-SiO_2(1173)	87.2	8.4	4.4	2.2	19.8

[a] Values calculated by the integrated intensities of the decomposed bands following Beutel et al. [11] $C_{Rh,tot} = \sum_j \frac{E_{i,j}}{\varepsilon_{i,j} x E_{i,T} x z(j)}$ where $E_{i,j}$ and $E_{i,T}$ are the integrated absorbances, $\varepsilon_{i,j}$ are the integrated extinction coefficients and $z(j)$ the strochiometric factors.
[b] Linearly bonded CO.
[c] Gem dicarbonyl CO.
[d] Bridge-bonded CO.

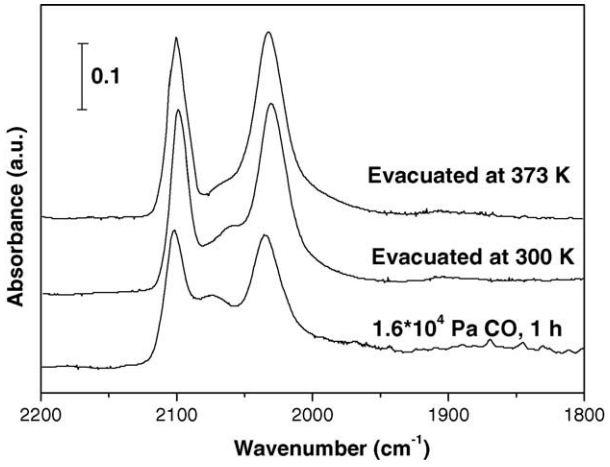

Fig. 6. Time evolution of the FTIR spectra of Rh (0.6%)/La_2O_3 (27%)-SiO_2 in the presence of CO.

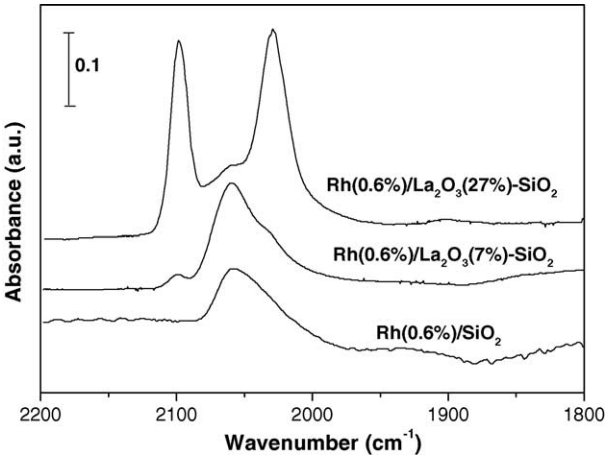

Fig. 7. FTIR of Rh catalysts after exposure to 1.6×10^4 Pa CO at 473 K.

decoration of the Rh° metal surface with promoter oxide patches so that the remaining ensembles are too small to accommodate bridging CO ligands. In some cases, increased L/B ratios have been observed with increasing metal dispersion [11]. The same authors claimed that the strong metal-promoter interaction (SMPI) state as induced by HT reduction increases the relative amount of linear to bridge CO. The L/B values of our La-Si solids could be partly due to the high metal–lanthanum interaction already found in Rh-La solids [15] and/or to the high metal dispersion.

3.4.2. Time evolution and evacuation of adsorbed CO species

An enhancement of the dicarbonyl bands was observed when CO remained in contact with Rh (0.6%)/La_2O_3 (27%)-SiO_2 for 1 h (Fig. 6). All the silica containing solids showed the same behavior, even though it was more significant for the lanthanum-silica catalysts. Evacuation at room temperature caused a reduction in the intensity of the band due to linear CO and a band shift to 2066 cm^{-1}. The gem-dicarbonyl species were resistant to desorption. The same trend was observed in all the solids. On Rh (0.6%)/SiO_2 (not shown) the linearly bonded CO band shifted to 2053 cm^{-1} while a weak band at 2099 cm^{-1} and a shoulder at 2025 cm^{-1} appeared. These bands could be attributed to the presence of small amounts of gem-dicarbonyls. Anderson et al. [9] observed that evacuation for 20 min caused that the dominant band at 2071 cm^{-1}, due to linearly adsorbed CO, shifted to 2058 cm^{-1}. The band shift may be ascribed to a decrease in dipole coupling between adjacent CO molecules combined with increased electron donation from rhodium to CO.

3.4.3. Adsorption at 473 K

Solymosi and co-workers [20] reported that in the presence of CO the $Rh^+(CO)_2$ species on silica support is transformed back into Rh_x-CO species at a higher temperature. This transformation took place only in the Rh (0.6%)/La_2O_3 (7%)-SiO_2 solid (Fig. 7), indicating the occurrence of the reductive agglomeration of highly dispersed Rh^+. This could be related to the low load of lanthanum in this solid. There was no full coverage of the silica surface with the lanthanum phase as can be observed from XRD and TPR results. As a consequence, there was O^{2-} on the silica available for the following reaction:

$$2Rh^+(CO)_2 + O^{2-} \rightarrow 2Rh^\circ\text{-CO} + CO + CO_2.$$

3.5. Physicochemical properties and catalytic behavior

It is well known that, among the noble metals, supported Rh is one of the most active and stable catalysts for the dry reforming of methane. The catalytic activity of Rh is strongly influenced by the nature of the support [15,22]. The turnover frequency (TOF) based on exposed Rh decreased with increasing rhodium dispersions [23]. It has been shown that lanthana can substantially modify the chemical behavior of M/SiO_2 systems [24] and their activity for several reactions [8]. The role of La_2O_3 as promoter on Rh-silica solids in the syngas production from CO_2 and CH_4 was explored by Gronchi et al. [25] using 5% La_2O_3-SiO_2 obtained by impregnation. They found a greater carbon deposition on lanthana-supported catalysts than on the silica ones. They claimed that the addition of lanthana activates the CO_2 dissociation and the carbon deposition. La_2O_3 would enhance the extent of methanation by supplying CO to the metal. Our catalysts did not show carbon deposition through TGA and LRS measurements. In the case of Rh/La_2O_3 catalysts, the strong interaction between Rh and La oxide is probably responsible for the high stability of these solids [14,15]. The chemical affinity of Rh and La_2O_3 to form rhodates could be the basis of the enhanced stability of the rhodium formulations. The rhodium–lanthana interaction is weaker in the La_2O_3-SiO_2 supported solids than in Rh/La_2O_3 (TPR), probably due to the lanthanum disilicate phase (XRD) formation. On the other hand, FTIR results indicate

that a partial decoration of the Rh metal particles could take place in the La_2O_3-SiO_2 supported catalysts. This Rh–La interaction would be strong enough to prevent the carbon deposition as was found to occur in the Rh/La_2O_3 solids [14,15].

An unusual catalytic stability was reported for Ni supported on lanthanum oxide. The tight coating of the nickel particles by layers of lanthanum carbonate could hinder the formation of deactivating coke. In our Rh/La_2O_3 samples, the presence of surface carbonate species was detected through XPS [15], and confirmed by the presence of the crystalline phase II-$La_2O_2CO_3$. However, in the La_2O_3-SiO_2 catalyts used in the membrane reactor, no lanthanum oxycarbonates were detected.

The metal dispersion is a critically important parameter in catalytic behavior. The high dispersion (Table 1) of the metal on the composite support would be responsible for the high-reaction rates of these solids. However, the TOF values decrease with the increasing dispersion of rhodium. The low TOF values suggest that the activity of the rhodium sites are lower than in the case of the Rh/La_2O_3 solids. Yokota et al. [23] correlated the different TOFs with the stabilized species of Rh atom using XAFS measurement. They concluded that the supports influenced the electronic state of Rh atoms, and that Rh metal catalysed the dry reforming reaction as a prominent active species. Further research is needed to study the differences between the Rh active sites on lanthanum-based catalysts, employing appropriate techniques such as XPS and TEM.

3.6. Membrane reactor

When highly hydrogen-selective membranes were used, improvement in the methane conversions were reported [1–4,26]. The silica membranes allowed a significant enhancement in the yields of H_2 and CO at atmospheric pressure. However, the results reported with Pd membranes employing Pt/Al_2O_3 catalysts showed an important carbon deposition.

Lund and co-workers [27] pointed out that the best way to compare the yield from a porous membrane reactor process to a plug flow reactor (PFR) is not obvious, since the two kinds of reactors are inherently different and it is important to make the comparison on the most equitable basis possible. In most of the research on equilibrium shifting, the yield from a membrane reactor was directly compared to the yield from a PFR that has reached thermodynamic equilibrium without considering the reactor geometry. Instead, in what follows we compare the Pd–Ag dense (non-porous) membrane reactor performance with the same reactor operated under fixed-bed conditions, i.e. with no differential pressure across the membrane, and no sweep gas flow through the permeate side.

Table 4 shows the catalytic behavior of Rh formulations in the membrane reactor. At 5.0×10^{-4} g h ml^{-1}, when the reactor was operated as a fixed-bed reactor, without sweep gas and without pressure drop, the methane and carbon dioxide conversions for Rh (0.2%) were lower than the theoretical equilibrium values (27.5 and 38.0, respectively) calculated considering the reverse WGS reaction.

Kikuchi et al. [5] sustained that the reverse water gas shift reaction can be avoided using a membrane with a higher rate of H_2 permeation than that of H_2 formation. They used Ni and some precious metal (Pd, Ru, Rh, Ir and Pt) supported on alumina. For these catalysts, they reported that the hydrogen formation was slower than the hydrogen permeation, so the RWGS was not important in the membrane reactor. However, the carbon formation led to catalyst deactivation.

In our case, when a sweep gas flow rate of 10 ml min^{-1} was used, both conversions were increased approximately by 30%. On the other hand, Rh (0.6%) solids started with equilibrium conversions. This is in agreement with the high TOF obtained for these solids.

Table 4
Catalyst comparison in a membrane reactor at 823 K

Catalysts	W/F[a] (g h ml^{-1})	Sweep gas (ml min^{-1})	$R_{CH_4}/R_{H_2 permeation}$[b] (non-dimensional)	X_{CH_4} (%)	X_{CO_2} (%)	Reaction equilibration ratio[c]	Permeate H_2 (mol h^{-1} m^{-2})
Rh (0.2%)/La_2O_3	5×10^{-4}	0		22.2	29.3	–	0.0
		10	2.7	29.0	38.6	nm	7.9
Rh (0.6%)/La_2O_3	3×10^{-4}	0		21.9	33.7	–	0.0
		10	1.8	28.9	39.9	nm	7.3
	5×10^{-4}	0		26.0	41.9	1	0.0
		10	3.0	33.9	41.0	0.43	10.1
Rh (0.6%)/La_2O_3 (27%)-SiO_2	3×10^{-4}	0		29.9	41.0	1	0.0
		10	3.0	32.3	42.8	0.76	8.3
	5×10^{-4}	0		30.4	41.7	1	0.0
		10	5	33.7	44.5	1	9.8

[a] The total reactant flow rate was 16.7 ml min^{-1}.

[b] Non-dimensional ratio: methane reaction rate/hydrogen permeation rate. The hydrogen permeation rate was measured with pure H_2 at 823 K and a ΔP = 20 kPa. Permeation area = 3×10^{-4} m^2.

[c] For the dry reforming reaction $\eta = \dfrac{\prod_i p_i^{\nu_i}}{K_{eq}}$.

Hughes [28] sustained that it is necessary to balance the feed rate, reaction rate and permeation rate for an optimal performance. It has been noted that for the optimal performance of a membrane reactor, the rate ratio ($R_{CH_4}/R_{H_2permeation}$) should take values between 0.1 and 10 [27–29]. This parameter accounts for the ability of the reactor to convert CH_4 and to transport H_2. The activity of the catalyst is important for equilibrium reactions. If the catalyst is of low activity, equilibrium is approached too slowly, so that removal of the hydrogen produced will not affect the yield. When Pd–Ag dense membranes are used, the permeation rate could be too low, then the system could behave as a conventional fixed-bed reactor. To decrease this ratio the permeation area should be increased.

For all our catalysts, a significant improvement in the methane conversion was obtained using the membrane reactor. In addition, the measured $R_{CH_4}/R_{H_2permeation}$ ratio values (between 1.8 and 5.0) were within the margins of good performance.

In the present work, an approach to compare different catalysts has been adopted. One can define a fraction of reaction equilibration for the carbon dioxide reforming reaction ($CH_4 + CO_2 \leftrightarrow 2CO + 2H_2$) using the following equation:

$$\eta = \frac{\prod_i p_i^{\nu_i}}{K_{eq}}$$

where p_i is the measured partial pressure of the reactants in the reaction side of the membrane reactor, ν_i the stoichiometric numbers for the $CO_2 + CH_4$ reaction and K_{eq} is the experimental equilibrium constant (evaluated in the fixed-bed reactor operation mode that is close to the theoretical value). If the composition corresponds to thermodynamic equilibrium these ratios will equal 1. A similar approach was proposed by Li et al. [29] for the simulation of the effects of continuous hydrogen removal and catalytic sites on CH_4 conversion to C_2H_4, and by Ma and Lund [30] in a water gas shift membrane reactor. This was accomplished through the mathematical simulation of the reactor.

Comparing the Rh (0.6%) catalysts at low $W/F = 5.0 \times 10^{-4}$ g h ml^{-1}, Table 4 shows that the La_2O_3 solid does not reach the equilibrium composition ($\eta = 0.43$), while the La_2O_3-SiO_2 catalyst exhibits a ratio equal to 1 and at lower W/F the ratio is 0.76.

To optimize the membrane reactor operation increasing the hydrogen permeation flux through the membrane, two main parameters were investigated: the sweep gas flow rate in the permeation side and the membrane permeation area. Fig. 8 shows the results obtained with the Rh solids in the membrane reactor when the sweep gas flow in the permeate side was changed. These experiments were carried out employing residence times that allowed thermodynamic equilibrium to be reached when the reactor was operated in the fixed-bed mode.

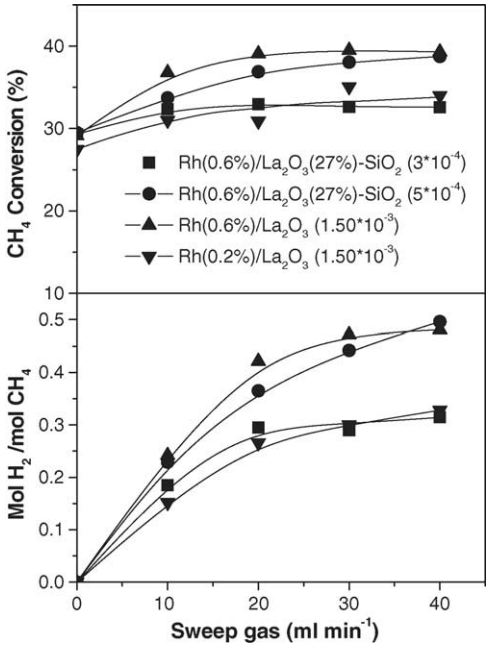

Fig. 8. Comparison of the effect of the sweep gas flow upon the membrane reactor performance for Rh solids evaluated at different residence times. $T = 823$ K, $\Delta P = 0$ Pa, W/F (g h ml^{-1}).

The increase of the Ar sweep gas flow rate reduces the hydrogen partial pressure in the permeate side leading to higher H_2 flow rate through the membrane; then, the permeated H_2 flow per mol of CH_4 fed in the reaction side increases (Fig. 8).

The Rh (0.6%)/La_2O_3 exhibits a greater equilibrium displacement and production of H_2 than the Rh (0.2%)/La_2O_3 (Fig. 7a) with the same residence time. Besides, the Rh (0.6%)/La_2O_3 (27%)-SiO_2 with a significantly lower W/F presents a performance similar to the Rh (0.6%) supported on lanthana. When a lower residence time was employed ($W/F = 3 \times 10^{-4}$ g h ml^{-1}), the results obtained with the Rh (0.6%)/La_2O_3 (27%)-SiO_2 were similar to those of the Rh (0.2%) with a five-times higher W/F.

The latter two solids present a similar behavior in the reaction equilibration ratio (Fig. 9): when the sweep gas flow increases this ratio decreases. For the Rh (0.6%)/La_2O_3, the reaction equilibration ratio begins to diminish when the sweep gas flow rate is higher than 30 ml min^{-1}. However, for the solid supported on the binary oxide operated at $W/F = 5 \times 10^{-4}$ g h ml^{-1}, the equilibration ratio changes very slowly. This is in agreement with the constant increase of methane conversion as a function of the sweep gas flow. In the other cases, both the conversion and the methane/hydrogen ratio remained practically constant. This would indicate that for the most active catalysts, it would be possible to obtain an increase in conversion if the sweep gas flow were increased even more. This behavior could be related to the good dispersion and high turnover frequency (Table 1) of the novel La_2O_3-SiO_2 solid.

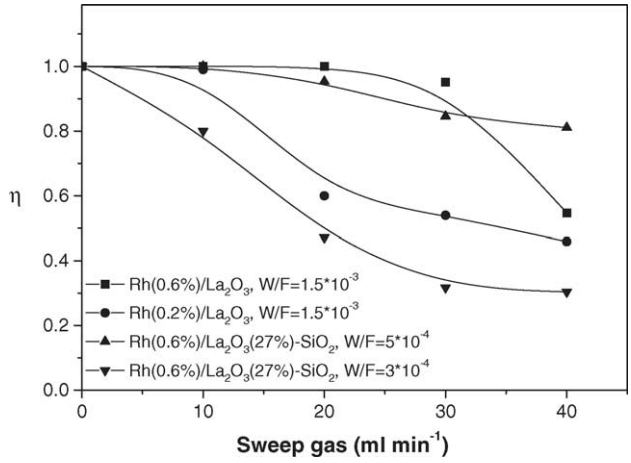

Fig. 9. Variation of the equilibration reaction ratio for the dry reforming reaction $\left(\eta = \frac{\prod_i p_i^{\nu_i}}{K_{eq}}\right)$ with the sweep gas flow rate evaluated at different residence times in the membrane reactor. $T = 823$ K, $\Delta P = 0$ Pa, W/F (g h ml^{-1}).

The effective permeation of the Pd–Ag membrane is another parameter that allows the modification of the hydrogen permeation flux. The effect of the contact area between the catalyst and the Pd–Ag membrane was studied. The Rh (0.6%)/La_2O_3 (27%)-SiO_2 catalyst was chosen due to its high dispersion and high methane reaction rate. Fig. 10 compares the catalytic behavior of the Rh (0.6%)/La_2O_3 (27%)-SiO_2 catalyst using two different effective permeation areas. The contact area was changed employing a different catalyst mass/quartz mass ratio in order to obtain the appropriate bed height. The permeation area was modified keeping the catalyst mass (W) and the total feed flow rate (F) constant. This implies that the contact time was the same in both experiments (Fig. 10).

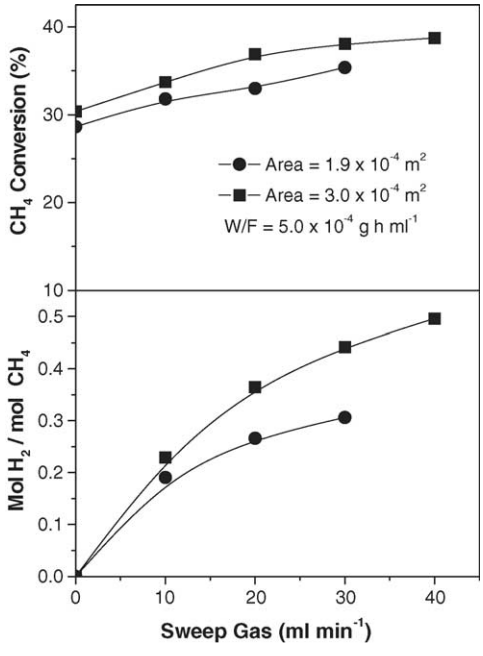

Fig. 10. Effect of the permeation area for Rh (0.6%)/La_2O_3 (27%)-SiO_2 in the membrane reactor.

In the membrane reactor, it is interesting to note that the methane conversion decreased by 10% diminishing the permeation area from 3×10^{-4} m^2 to 1.9×10^{-4} m^2, while the same amount of catalyst and the same reactant flow rate were used. In consequence, the hydrogen permeation flux decreased. As expected, the effective permeation area is an important factor that affects the performance of the membrane reactor.

In a previous paper, we studied the effect of pressure [6] over a small range (0–80 kPa). The negative effect of pressure over CO_2 and CH_4 conversions was dominant and the hydrogen flux remained constant with an increase of pressure drop through the membrane.

In a recent paper, Oyama and co-workers [26] studied the effect of pressure in a membrane reactor containing a hydrogen-selective silica membrane at non-equilibrium conditions. They demonstrated that the RWGS reaction was very fast and reached equilibrium while the reforming reaction always operated below equilibrium. When the reaction was carried out at pressures between 1 and 20 atm, the yield of hydrogen in the membrane reactor at first rose with pressure, but then dropped because of the unfavorable equilibrium and enhanced rate of the reverse reaction.

After testing several catalysts for more than 1000 h on stream, H_2 permeability measurements were performed to verify that the membrane had not changed during the reaction. No visual damage or carbon deposition were observed and the membrane did not show any variation on the hydrogen permeation rate. Furthermore, for all the used catalysts reported in the present paper, no carbon deposition was observed through TGA measurements. However, a small amount of graphitic carbon was detected using laser Raman spectroscopy [7].

4. Conclusions

- The La-containing Rh catalysts are very stable under reaction conditions while the presence of tiny amounts of graphite only detectable through LRS does not endanger membrane stability.
- The strong metal-support interaction (TPR) in Rh/La_2O_3 catalysts is the basis of their high stability. The La_2O_3-SiO_2 solids are also stable, even though a weaker rhodium–lanthanum interaction (TPR) is observed. In the same way, the linear to bridge CO band ratio was slightly higher in the La_2O_3-SiO_2 solids confirming the presence of the Rh–La interaction.
- The incorporation of the promoter (La_2O_3) to the silica support induces a parallel increase in the metal dispersion. The slight blue-shift of the linear CO bands would be related to the high dispersion observed. The concentration of surface Rh atoms slightly increases with lanthanum addition.

- For all our catalysts, a significant improvement in the methane conversion was observed in the membrane reactor but the best performing formulation was obtained using the composite La_2O_3-SiO_2 support. For the Rh (0.6%)/La_2O_3 (27%)-SiO_2 catalyst, the reaction equilibration ratio remained constant with the increase of the sweep gas flow.

Acknowledgements

The authors wish to acknowledge the financial support received from UNL, CONICET and ANPCyT. They are also grateful to the Japan International Cooperation Agency (JICA) for the donation of the major instruments used in this study. Thanks are given to Elsa Grimaldi for the English language editing and to Marcos Kihn and Alejandro Roa for their technical assistance.

References

[1] J. Galuszka, R. Pandey, S. Ahmed, Catal. Today 46 (1998) 83.
[2] P. Ferreira-Aparicio, I. Rodríguez-Ramos, A. Guerrero-Ruiz, Appl. Catal. A 237 (2002) 239.
[3] B.S. Liu, C.T. Au, Catal. Lett. 77 (2001) 67.
[4] A.K. Prabhu, R. Radhakrishnan, S. Ted Oyama, Appl. Catal. A 183 (1999) 241.
[5] E. Kikuchi, Y. Chen, Stud. Surf. Sci. Catal. 107 (1997) 547.
[6] J. Múnera, S. Irusta, L. Cornaglia, E. Lombardo, Appl. Catal. A 245 (2003) 383.
[7] L.M. Cornaglia, J. Múnera, S. Irusta, E. Lombardo, Appl. Catal. A 263 (2004) 91.
[8] H. Vidal, S. Bernal, R. Baker, G. Cifredo, D. Finol, J.M. Rodriguez Izquierdo, Appl. Catal. A 208 (2001) 111.
[9] J. Anderson, C. Rochester, Z. Wang, J. Mol. Catal. A 139 (1999) 285.
[10] R. He, H. Kusaka, M. Mavrikakis, J. Dumesic, J. Catal. 217 (2003) 209.
[11] T. Beutel, O. Alekseev, Y. Rydin, V. Likholobov, H. Knòzinger, J. Catal 169 (1997) 132.
[12] S. Bernal, G. Blanco, J. Calvino, M. Rodríguez-Izquierdo, H. Vidal, J. Alloys Compd. 250 (1997) 461.
[13] H. Vidal, S. Bernal, R. Baker, D. Finol, J.A. Perez Omil, J.M. Pintado, J.M. Rodriguez Izquierdo, J. Catal. 183 (1999) 53.
[14] S. Irusta, L. Cornaglia, E. Lombardo, Mater. Chem. Phys. 86 (2004) 440.
[15] S. Irusta, L. Cornaglia, E. Lombardo, J. Catal. 210 (2002) 7.
[16] A. Borer, R. Prins, J. Catal. 144 (1993) 439.
[17] C. Crisafulli, S. Scire, R. Maggiore, S. Minico, S. Galvagno, Catal. Lett. 59 (1999) 21.
[18] P. Basu, D. Panayotov, J.T. Yates, J. Am. Chem. Soc. 110 (1988) 2074.
[19] R.A. Van Santen, in: H.H. Brongersma, R.A. Van Santen (Eds.), Fundamental Aspects of Heterogeneous Catalysis Studied by Particle Beams, Plenum, New York, 1991, p. 83.
[20] E. Novák, D. Sprinceana, F. Solymosi, Appl. Catal. A 149 (1997) 89.
[21] G. Gallaher, J. Goodwin, C. Huang, M. Houalla, J. Catal. 140 (1993) 453.
[22] U.L. Portugal, A.C.F. Santos, S. Damyanova, C.M.P. Marques, J.M.C. Bueno, J. Mol. Catal. A: Chem. 184 (2002) 311.
[23] S. Yokota, K. Okumura, M. Niwa, Catal. Lett. 84 (2002) 131.
[24] R. Kieffer, A. Kiennemann, M. Rodriguez, S. Bernal, J.M. Rodriguez-Izquierdo, Appl. Catal. 42 (1988) 77.
[25] P. Gronchi, P. Centola, R. Del Rosso, Appl. Catal. A: Gen. 152 (1997) 83.
[26] D. Lee, P. Hacarlioglu, S.T. Oyama, Top. Catal. 29 (2004) 45.
[27] C. Reo, L. Bernstein, C. Lund, Chem. Eng. Sci. 52 (1997) 3075.
[28] R. Hughes, Membr. Technol. 131 (2001) 9.
[29] L. Li, R. Borry, E. Iglesia, Chem. Eng. Sci. 57 (2002) 4595.
[30] S. Ma, C. Lund, Ind. Eng. Chem. Res. 42 (2003) 711.